energies

MDPI

Article

Analysis and Design of Fuel Cell Systems for Aviation

Thomas Kadyk [1,*], Christopher Winnefeld [2], Richard Hanke-Rauschenbach [2] and Ulrike Krewer [1]

[1] Institute of Energy and Process System Engineering, TU Braunschweig, Franz-Liszt Str. 35, 38106 Braunschweig, Germany; u.krewer@tu-braunschweig.de

[2] Institute of Electric Power Systems, Gottfried Wilhelm Leibniz Universität Hannover, Welfengarten 1, 30167 Hannover, Germany; christopher.winnefeld@ifes.uni-hannover.de (C.W.); hanke-rauschenbach@ifes.uni-hannover.de (R.H.-R.)

* Correspondence: t.kadyk@tu-braunschweig.de; Tel.: +49-391-531-3037

Received: 21 December 2017; Accepted: 31 January 2018; Published: 6 February 2018

Abstract: In this paper, the design of fuel cells for the main energy supply of passenger transportation aircraft is discussed. Using a physical model of a fuel cell, general design considerations are derived. Considering different possible design objectives, the trade-off between power density and efficiency is discussed. A universal cost–benefit curve is derived to aid the design process. A weight factor w_P is introduced, which allows incorporating technical (e.g., system mass and efficiency) as well as non-technical design objectives (e.g., operating cost, emission goals, social acceptance or technology affinity, political factors). The optimal fuel cell design is not determined by the characteristics of the fuel cell alone, but also by the characteristics of the other system components. The fuel cell needs to be designed in the context of the whole energy system. This is demonstrated by combining the fuel cell model with simple and detailed design models of a liquid hydrogen tank. The presented methodology and models allows assessing the potential of fuel cell systems for mass reduction of future passenger aircraft.

Keywords: aviation; hydrogen; fuel cell; systems design

1. Introduction

In the realm of the global energy crisis and climate change, the aviation sector is a significant player. Since the 1980s, CO_2 emissions from aviation have increased by 3.6% per year, i.e., twice the world's total growth rate [1]. As a result, aviation currently accounts for 12% of transport-related CO_2 emissions and 2–3% of all anthropogenic emissions [2] with a steadily increasing influence. In order to tackle this challenge, the European Commission formulated reduction targets in the "Flight Path 2050": 75% CO_2 reduction per passenger kilometre relative to the capabilities of typical new aircraft in 2000, as well as 90% NO_x and 65% perceived noise reduction [3]. Similarly, two US government agencies, the International Air Transport Association (IATA), and the International Civil Aviation Organization (ICAO), pursue an average improvement in fuel efficiency of 1.5% per year until 2020, a cap on net aviation CO_2 emissions from 2020 (carbon-neutral growth) and a 50% CO_2 reduction until 2050 [2].

Considering the increasing amount of air travel, these goals are unlikely to be reached by evolutionary improvement of existing aviation technology. Recently, Müller et al. analysed the influence of modern, fuel efficient aircraft and retrofit options on fleet planning and fleet emissions [4]. The latest generation of aircraft has 15% less fuel burn by using geared turbofans and composite materials. Retrofit options of existing aircraft yield 9–12% less fuel burn by using blended winglets, cabin weight reduction, electric taxing, or re-engining. A low-cost carrier as well as a full service network carrier were analysed. While moderate CO_2 emission reductions of 12% and 7% compared to

the "business as usual" scenario could be achieved with such measures, the overall CO_2 emissions are predicted to increase further until 2025.

A tenable solution would be the use of hydrogen as fuel, as already pointed out at the end of the 1970s by Bockris and Justi [5] and references therein. Because of its three times higher gravimetric energy density, using hydrogen can reduce overall weight of the aircraft. This effect is pronounced in fuel-intensive aircraft like long-distance, large passenger number, and hypersonic aircraft [5–8]. Once hydrogen is used as a fuel, there is no better converter than a fuel cell. The increased efficiency of a fuel cell leads to a further reduction of the fuel load. Fuel cells enable further advantages of electric aircraft such as distributed propulsion, which increases the aerodynamic efficiency. Furthermore, multifunctional integration of the fuel cell into aircraft via harvesting by-products, such as water, heat or oxygen-depleted exhaust air, allows for using the fuel cell to provide vital processes like de-icing, cabin air conditioning, water supply or fire suppression of luggage compartment or fuel tanks [9].

Besides fuel cell and hydrogen tank, fuel cell systems are composed of various auxiliary components for media and heat management. These components and their arrangement influence efficiency and weight as well. As in automotive applications, a good system design minimises weight, complexity and number of system components, while assuring operation over the whole load range and high efficiencies [10]. Robustness to the strongly changing environmental conditions, especially temperature and humidity of air inlet, are furthermore crucial. Model-based analysis allows a systematic evaluation and quantification of effects of environmental conditions [11] and of process integration for weight minimisation [12]. Assessing the wide range of system design options is out of scope of this work; instead, the fuel cell is designed in the context of the whole system.

In order to design fuel cell systems for aviation, this article starts with general design considerations for fuel cells derived from the analysis of a physical model of a polymer electrolyte membrane fuel cell (PEMFC). It can be seen that the PEMFC can be designed to optimize performance, thus minimizing the size of the fuel cell, or can be designed to increase efficiency, thus minimizing fuel consumption and the size of the fuel tank and other system components like air supply compressors.

These design considerations are then applied to design fuel cell systems for the main energy supply of passenger transport aircraft. Starting with simplified models of fuel cell and tank, the design principles are explored. Since the optimum fuel cell design depends on the characteristics not only of the fuel cell but also of the other systems components, the model is refined by a more detailed liquid hydrogen tank model. In this tank model, the energy density is maximised for a specific operation profile, i.e., flight mission. In addition, estimates of future developments in lightweight fuel cells are discussed. With these advanced technologies, the potential of fuel cell systems in future aircraft is assessed.

2. Model

This analysis employs a PEMFC model that is as simple as possible while still covering all relevant processes in physically meaningful, macroscopic parameters. The charm of the model is that Andrei Kulikovsky was able to obtain an approximate but accurate analytical solution [13]. This has three main advantages: (1) the functional relationship between parameters and interesting variables is directly revealed; (2) the model has no computational limitations and can be included into larger model hierarchies, e.g., for aircraft design, aircraft fleet models or future aviation scenario modelling; and (3) the effective, physical parameters of the model can be used to estimate the improvements due to future materials' development.

In the model, the main losses of the fuel cell stem from the cathode catalyst layer (CCL). The ohmic losses are combined into one ohmic resistance, R_Ω, which covers membrane, electric, and contact resistances. The anode losses are considered negligible.

For the cathode performance, a well known model based on pioneering works of Perry, Newman and Cairns [14] as well as Eikerling and Kornyshev [15] is used. The model consists of governing

equations for the rate of the oxygen reduction reaction (ORR) in the cathode catalyst layer, i.e., electrochemical current generation,

$$\frac{\mathrm{d}j}{\mathrm{d}x} = i_* \left(\frac{c}{c_{\mathrm{ref}}}\right) \exp\left(\frac{\eta}{b}\right), \tag{1}$$

Ohm's law for proton conduction,

$$-\sigma_{\mathrm{t}} \frac{\mathrm{d}\eta}{\mathrm{d}x} = j, \tag{2}$$

with σ as ionic conductivity, as well as oxygen diffusion through gas diffusion layer (GDL) and CCL,

$$D \frac{\mathrm{d}c}{\mathrm{d}x} = \frac{j_0 - j}{4\mathrm{F}}. \tag{3}$$

Here, j is the local proton current density, x is the distance from the membrane, i_* is the volumetric exchange current density (per unit CCL volume, A cm^{-3}), c is the local oxygen concentration c_{ref} is its reference (inlet) concentration, η is the local overpotential, b is the Tafel slope, σ_{t} is the CCL proton conductivity and j_0 and η_0 are the cell current density and cell overpotential, respectively.

This CCL model is 1D in through-plane direction and solved in steady-state under isothermal conditions. It is valid for large overpotentials, $\eta \gg b$. Since the diffusion coefficients in CCL and GDL, i.e., D and D_{b}, are effective parameters, polarization curves for flooded conditions can be simulated. However, a changing water balance, i.e., a dependency of the diffusion coefficients on current, is not modelled in detail here. Under these assumptions, Kulikovsky [13] was able to obtain the analytical solution for the polarization curve $\eta_0(j_0)$,

$$\begin{aligned} \eta_0 &= b \operatorname{arcsinh}\left(\frac{(j_0/j_\sigma)^2}{2(c_{\mathrm{h}}/c_{\mathrm{ref}})(1-\exp(-j_0/(2j_*)))}\right) \\ &+ \frac{\sigma_{\mathrm{t}} b^2}{4\mathrm{F}Dc_{\mathrm{h}}} \left(\frac{j_0}{j_*} - \ln\left(1 + \frac{j_0^2}{j_*^2\beta^2}\right)\right) \left(1 - \frac{j_0}{j^*_{\mathrm{lim}}(c_{\mathrm{h}}/c_{\mathrm{ref}})}\right)^{-1} \\ &- b \ln\left(1 - \frac{j_0}{j^*_{\mathrm{lim}}(c_{\mathrm{h}}/c_{\mathrm{ref}})}\right) \end{aligned} \tag{4}$$

with the three characteristic current densities

$$j_* = \frac{\sigma_{\mathrm{t}} b}{l_{\mathrm{t}}}, \tag{5}$$

$$j_\sigma = \sqrt{2 i_* \sigma_{\mathrm{t}} b}, \tag{6}$$

$$j^*_{lim} = \frac{4\mathrm{F}D_{\mathrm{b}}c_{\mathrm{h}}}{l_{\mathrm{b}}}, \tag{7}$$

where l_{t} and l_{b} are the thickness of CCL and GDL, respectively. The parameter β is a solution to the equation $\beta \tan(\beta/2) = j_0/j_*$, which can be accurately approximated by [13]

$$\beta = \frac{\sqrt{2(j_0/j_*)}}{1 + \sqrt{1.12(j_0/j_*)}\exp(\sqrt{2(j_0/j_*)})} + \frac{\pi(j_0/j_*)}{2 + (j_0/j_*)}. \tag{8}$$

The first term on the right-hand side of Equation (5) gives the overpotential due to the combined effect of ORR activation and proton transport. The second and third terms describe the potential losses due to oxygen transport in the CCL and GDL, respectively.

With Equation (5), the cell voltage V_{cell} can be calculated as

$$V_{\mathrm{cell}} = V_{\mathrm{oc}} - \eta_0 - R_\Omega j_0, \tag{9}$$

where V_{oc} is the open circuit voltage. The power density,

$$P = V_{cell} j_0, \tag{10}$$

and electric efficiency,

$$v = \underbrace{\frac{\Delta G}{\Delta H}}_{\substack{\text{thermodynamic} \\ \text{efficiency}}} \cdot \underbrace{\frac{V_{cell}}{V_{eq}}}_{\substack{\text{voltage} \\ \text{efficiency}}}, \tag{11}$$

complete the set of equations used in the analysis.

In addition to the fuel cell with mass m_{fc}, the mass of the fuel, m_{H_2} and of the fuel tank, m_{tk} are considered. Since the scaling relation for the mass of the tank depends on its geometry, the limiting case of a spherical tank, i.e., the smallest surface-to-volume ratio, is considered. In a first step, a constant area-specific mass ϱ_{tk} (unit kg m^{-2}) of the walls of the tank is assumed. With the derivation of m_{tk} in Appendix A, the total mass of the fuel cell system is

$$\begin{aligned} m_{tot}(P, v) &= m_{fc} + m_{tk} + m_{H_2} \\ &= \frac{P_{rq}}{\rho_{fc}} \frac{P_{max}}{P} + \varrho_{tk} (\pi)^{\frac{1}{3}} \left(6 \frac{E_{rq}}{\omega_{H_2} v \rho_{H_2}} \right)^{\frac{2}{3}} + \frac{E_{rq}}{\omega_{H_2} v}, \end{aligned} \tag{12}$$

where P_{rq} and E_{rq} are the required output power and energy, respectively. P is the power at which the cell is operated, P_{max} is the maximum power of the cell at the maximum power point (MPP), i.e., P_{max}/P is the oversizing factor of the fuel cell. ρ_{fc} is the specific power of the fuel cell system including peripheral components at maximum net output power in kW/kg. This way, ρ_{fc} implicitly includes the mass of peripheral components (like compressors, pumps, valves, etc.) and their parasitic power demand. ω_{H_2} is the specific energy of hydrogen, 33.3 kWh/kg, i.e., E_{rq}/v is the energy that needs to be stored in the tank.

In a second step, a more detailed tank model from Winnefeld et al. [16] was substituted. This model uses the equation of state of Leachman et al. [17] to describe the properties of the stored hydrogen. Modules for geometrical, mechanical and thermal design are combined with a study mission. With this, the geometry, wall thickness and insulation thickness can be dimensioned. For the comparison in this paper, again a spherical geometry is chosen as a limiting case. The other parameters and the mid-range study mission are taken as described in [16]. For a detailed description and discussion of the model and design process, the reader is referred to [16]. All models were implemented in MATLAB® (MathWorks, Natick, MA, USA) using the parameters given in Table 1.

Table 1. Model parameters used.

Parameter	Value	Reference
GDL thickness l_b	250 µm	[13,18]
CCL thickness l_t	10 µm	[13,18]
Membrane thickness l_m	25 µm	[13,18]
oxygen concentration c_h (p = 1 bar)	7.36×10^{-6} mol cm^{-3}	[13]
Cell open-circuit potential V_{oc}	1.145 V	[13,18]
CCL proton conductivity σ	0.03 S m^{-1}	[13]
Tafel slope b	0.03 V	[13]
exchange current density i_*	0.817×10^{-3} A cm^{-3}	[13]
effective diffusion coefficient of GDL D_b	0.0259 cm^2 s^{-1}	[13]
effective diffusion coefficient of CCL D	1.36×10^{-4} cm^2 s^{-1}	[13]

Table 1. *Cont.*

Parameter	Value	Reference
required energy for flight mission, E_{rq}	63.7 MWh	[16]
required power of current aircraft, P_{rq}	27.6 MW	[19]
required power of future aircraft, P_{rq}	16.3 MW	[19]
area-specific tank mass, ϱ_{tk}	75 kg m^{-2}	[20]
specific power of fuel cell+periphery (currently), ρ_{fc}	1.6 kW kg^{-1}	[21]
specific power of fuel cell+periphery (future), ρ_{fc}	8 kW kg^{-1}	estimate
specific power of electric motor (currently), ρ_{em}	5.2 kW kg^{-1}	[22]
specific power of electric motor (future), ρ_{em}	10 kW kg^{-1}	estimate

GDL = gas diffusion layer; CCL = cathode catalyst layer.

3. Results and Discussion

3.1. General Design Considerations

Figure 1 shows the typical behaviour of a PEFC in the form of polarisation curve and power curve. Via Equation (11), the polarisation curve can directly be transformed into an efficiency curve. For aircraft design, efficiency and power density of the fuel cell are the two main performance parameters. The efficiency determines the weight of the fuel that is needed. The power density determines the weight of the fuel cell. Hence, it is beneficial to plot the functional relation between both objectives, as shown in Figure 2.

By selecting the operating point, one can move along this "performance map". The operating point can be designed in two limiting ways: for a given fuel cell size, by setting the current, voltage or output power; or for a given current, voltage or power requirement, by (over-)sizing the fuel cell. The curve in Figure 2 is bistable, i.e., two possible operating points can give the same output power. For all practical purposes, the operating point with the higher efficiency is preferable, i.e., the fuel cell should always be operated at currents below or up to the MPP. For ease of comparison, the unpreferred low efficiency branch is marked with a dotted line in all following figures.

The general trend of the high efficiency branch in Figure 2 is that by decreasing the power, i.e., operating at partial load or oversizing the fuel cell, the efficiency increases. This efficiency gain by load reduction, shown in Figure 3, is roughly constant at medium loads. However, close to equilibrium, i.e., in the activation region, and close to maximum power, reducing the power gains relatively high efficiency improvements. For practical purposes, the efficiency gain in the activation region is irrelevant because a fuel cell producing no current is useless. However, especially in the high power region, the efficiency gain asymptotically reaches infinity at the MPP, i.e., a slight power reduction gains a large efficiency increase. This suggests that the fuel cell should always be at least slightly oversized. Depending on the application, further oversizing, i.e., investing in a bigger and heavier fuel cell in order to gain a more efficient process, might be beneficial. To aid such decision, Figure 3 can be used as a performance cost–benefit curve. A remarkable property of this curve is that it is insensitive to variations of all design parameters of the model. A 10-fold increase and decrease of j_0, D, D_b, σ, l_t, l_b, c_h have been tested but show no visible change of the curve. To further illustrate this point with practical data, 41 polarisation curves from Ref. [23] have been analysed in the described fashion. The grey curves in Figure 3 mark the average value and the 99% confidence interval (i.e., a measured point has a 99% probability of lying within this interval) of the analysed experimental curves. The relatively narrow confidence region demonstrates the fundamental nature of this cost–benefit curve, which makes it a valuable design tool.

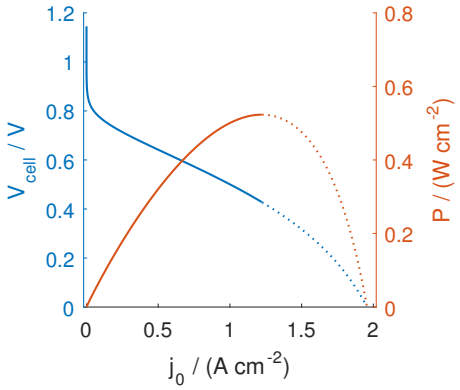

Figure 1. Polarisation curve (blue) and power curve (red) of a plymer electrolyte membrane fuel cell. Dotted line marks the high current branch above the maximum power point.

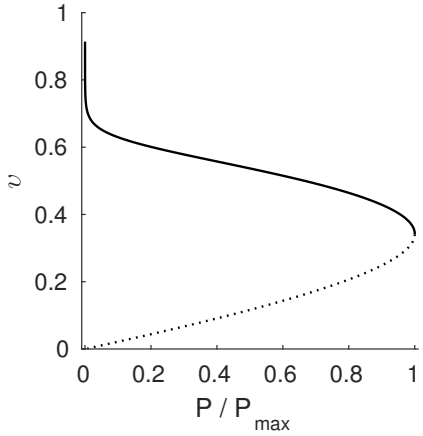

Figure 2. Cell efficiency vs. normalized cell power. Dotted line marks the high current branch above the maximum power point.

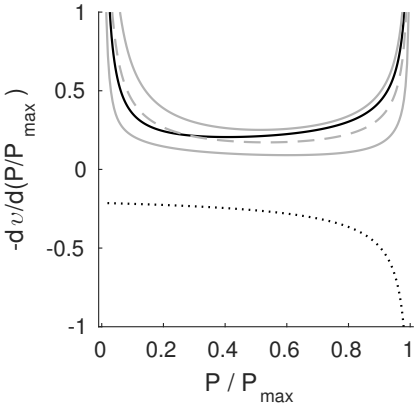

Figure 3. Efficiency gain that is obtained from lowering the power as function of operating power. The dotted line marks the branch above the maximum power point. Analysis of 41 experimental polarization curves [23] is marked in grey: the dashed line marks the average and the grey solid line mark the 99% confidence interval.

The question remains: How much should the fuel cell be oversized? In order to find the optimum operating point on the efficiency vs. power curve, the requirements of the application need to be brought into play. In the simplest case, a weight parameter w_P can be used, which defines the relative

importance of fuel cell power density vs. efficiency. With this weight, an overall objective function f can be calculated as

$$f(v, P) = w_P P + (1 - w_P)v. \quad (13)$$

Figure 4 shows this objective function for different weights w_P. For $w_P = 1$, i.e., only the fuel cell power density is important for the specific application, the objective function follows the power curve and the optimum lies at the MPP. For $w_P = 0$, i.e., only efficiency is important, the objective function follows the polarization curve and the optimum is at equilibrium. In between those two limits, the objective function transitions between power and polarization curve. During this transition from power to polarization curve, i.e., from $w_P = 1$ to $w_P = 0$, at first two optima/maxima exist: a local maximum at equilibrium that increases, and a global maximum near the MPP that decreases. When w_P is lowered to $w_P = 0.37$, both maxima have the same value. When lowering w_P further, the maximum at equilibrium becomes the global maximum. Since the maximum at equilibrium is practically irrelevant, the second characteristic transition at $w_P = 0.18$ (red dashed curve) is more important: here, the local maximum close to the MPP disappears and only the maximum at equilibrium remains.

In many applications, w_P might not be a simple constant and the objective might not depend linearly on efficiency and power density (cf. Equations (12) and (13)). Via w_P, not only technical but also nontechnical design objectives, like economic, ecological, social or political factors, can be coupled into the design process. Examples are system mass and volume, fuel consumption and emissions, direct operating costs, carbon tax, emission targets or restrictions, social acceptance or technology hype and more.

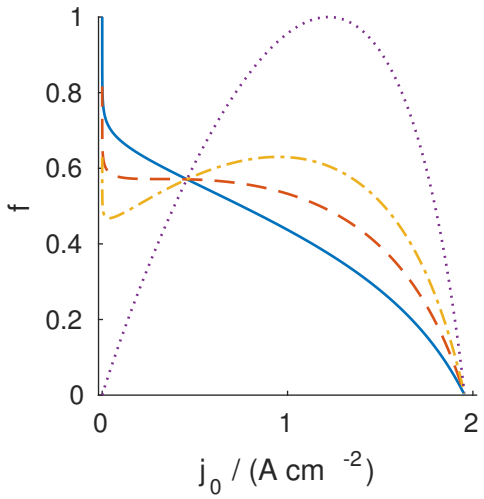

Figure 4. Objective function of power vs. efficiency optimization for 4 different weights. Dotted: $w_P = 1$, dash-dotted: $w_P = 0.37$, dashed: $w_P = 0.18$, solid $w_P = 0$.

3.2. Design for Passenger Aircraft

A primary design objective for aircraft is the overall weight. To estimate the fuel cell system mass, it can be assumed that the fuel cell mass scales linearly with output power. As an example, a scaling with 0.1 kg/kW is chosen, corresponding to future lightweight, high-power fuel cells discussed in the next section. For the tank, a spherical geometry can be assumed as a limiting case with the lowest surface-to-volume ratio. In stationary cryostatic hydrogen tanks, the walls have a typical specific weight of 75 kg/m^2 [20].

With this, the system and component masses result as depicted in Figure 5. As can be seen, the minimum system mass is not reached at the maximum power point of 1.22 A cm^{-2}, but when running the fuel cell at a significantly lower current density of 0.77 A cm^{-2}. The location of the

minimum depends on the trade-off between fuel cell mass and tank system mass. It is determined not only by the fuel cell characteristics, but also by the characteristics of the tank and other components of the systems. Hence, the fuel cell has to be designed in the context of the overall system. For the fuel cell design, it is not sufficient to consider a fuel cell model alone, but the models of the other system components determine the optimum fuel cell design as well.

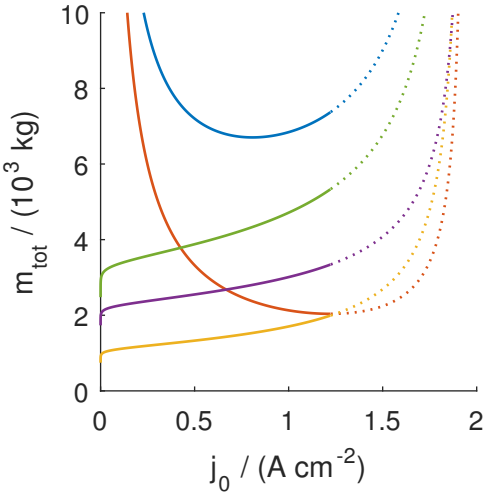

Figure 5. Mass of the fuel cell system and its components as function of working point current density for a reference flight mission with a power demand of P_{rq} =16.3 MW and an energy demand of E_{rq} = 63.7 MWh, i.e., a medium haul flight [16]. Blue: total mass of the system; Red: mass of the fuel cell; Yellow: mass of the hydrogen fuel; Purple: mass of the empty tank; Green: mass of the tank system (tank+hydrogen). Dotted lines mark the branch above the maximum power point.

To analyze the trade-off between fuel cell and tank system mass further, the dependency of the location of the minimum is derived. This trade-off can be described by the storage-converter ratio

$$r_{\mathrm{s/c}} = \frac{E_{\mathrm{rq}}}{P_{\mathrm{rq}}} \cdot \frac{\rho_{\mathrm{fc}}}{e_{\mathrm{tk}}} = \frac{m_{\mathrm{s}}}{m_{\mathrm{c}}}, \tag{14}$$

where the first term is the ratio of required energy, E_{rq}, and required power, P_{rq}. This term serves as an input parameter describing the design of the particular application. The second term is the ratio of the specific power of the energy converter, ρ_{fc}, and the specific energy of the energy storage, e_{tk}. This term covers the characteristics of the system components, i.e., ρ_{fc} is a function of the fuel cell parameters and e_{tk} is a function of the tank parameters. More generally speaking, the dimensionless $r_{\mathrm{s/c}}$ can also be understood as the ratio of storage-to-converter mass.

The location of the minimum in Figure 5 can be described using the factor by which the fuel cell needs to be oversized in order to minimize the system mass,

$$r_{\mathrm{os}} = \frac{P_{\mathrm{max}}}{P_{\mathrm{rq}}}. \tag{15}$$

The relationship between r_{os} and $r_{\mathrm{s/c}}$ is shown in Figure 6, where the red curve marks the spherical tank design mentioned above. The semi-logarithmic plot reveals that for this design, the optimal oversize grows exponentially with $r_{\mathrm{s/c}}$ for systems with $r_{\mathrm{s/c}} > 1$, i.e., systems with dominating storage weight. For systems with $r_{\mathrm{s/c}} < 0.5$, i.e., systems with dominating converter weight, oversizing is negligible. The blue curve shows a more complex tank design discussed in the next section. This tank system allows for venting of hydrogen, which seems to shift the curve towards higher $r_{\mathrm{s/c}}$ but keeps the exponential relationship between r_{os} and $r_{\mathrm{s/c}}$ for $r_{\mathrm{s/c}} > 4$.

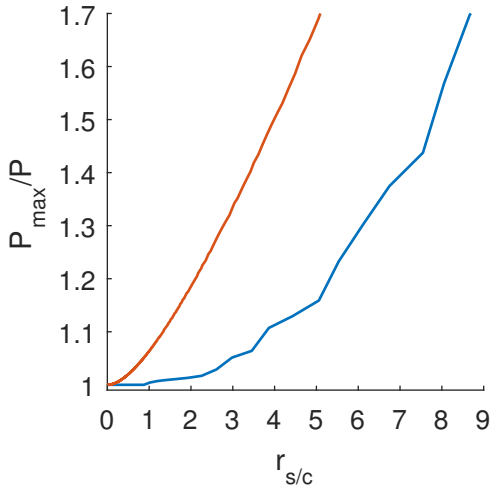

Figure 6. Fuel cell oversize for minimum fuel cell system weight as function of the ratio of tank-to-fuel cell mass. Red: Stationary tank design. Blue: Advanced tank design of Winnefeld et al. [16].

3.3. Sensitivity Analysis for Future Aircraft

Considering the fundamental finding that for designing the fuel cell the whole system needs to be taken into account, a more detailed tank design from Winnefeld et al. [16] was used for further analysis. In Winnefeld's design process, the tank design is tailored towards a specific flight mission profile. This takes advantage of the following synergies: in a liquid hydrogen tank, the heat flow from the environment into the tank would lead to a boil-off of hydrogen and thus an increase in pressure. To counter this effect, hydrogen can be extracted from the cell. Furthermore, the heat flow into the tank can be minimized by increasing the insulation or adding active cooling. Both of the latter measures would increase the system's mass. However, if the extracted hydrogen compensates the incoming heat flow at all times, these measures are unnecessary. If the hydrogen extraction overcompensates the heat flow, the insulation could even be reduced. In aircraft operation, sufficient extraction of hydrogen happens during all phases of the flight; the holding times on the ground before and after the flight with little or no hydrogen extraction are critical and determine the tank design [16]. However, minimizing holding times and thus turnaround times is also in the interest of air traffic management.

Winnefeld's design routine maximizes the energy density of the tank for a desired flight mission profile and determines the corresponding tank size, wall thickness, insulation thickness and hydrogen venting regime. The total mass of the optimized tank for a mid-range mission is 729 kg, which is significantly lower than the 2805 kg unoptimized stationary tank at the minimum in Figure 5. However, in both cases, the tank system (tank+hydrogen, i.e., 2719 kg and 4795 kg, respectively) is lighter than the kerosene that current aircraft would require for this flight mission (63.7 MWh = 5358 kg kerosene).

Similar to the tank technology, today's fuel cells still have room for improvement in mass and specific power. Such a development towards ultra-lightweight application is currently not strongly pursued because fuel cells are mostly developed with automotive applications in mind. In automotive fuel cells, the power density targets, e.g., of the US Department of Energy [24], are already reached and research focuses on reducing platinum loading, costs and size, as well as improving lifetime.

In order to estimate the potential for future fuel cells power density, let us consider the active components of a fuel cell, i.e., the membrane electrode assembly (MEA). Today, MEAs consist of a Nafion membrane (50 g m^{-2}) covered with Pt catalyst ink (4 g m^{-2} Pt + 10 g m^{-2} Carbon + 10 g m^{-2} ionomer) and a gas diffusion layer (e.g., Toray TGP-H-030, 44 g m^{-2}). This adds to about 100–200 g m^{-2} of MEA. Considering typical power densities of 1.5 W cm^{-2}, power densities in the range of 100 kW/kg_{MEA} are achieved. This number is likely to improve further with the development of new electrocatalysts, which showed a tremendous performance increase in the past while still having large room for improvement [25]. On the lab scale, power densities of <4 W cm^{-2} are already

achieved, e.g., by direct deposition of even thinner membranes onto the catalyst [26]. This increases the MEA power density further by a factor 3. However, the "passive" components of the fuel cell reduce the power density to 2 kW/kg on the stack level [27] and 1.6 kW/kg on the system level [21].

The most important of these "passive" components are the bipolar plates, which account for around 80% of the weight of a fuel cell stack [28]. Nowadays, bipolar plates are made of graphite–polymer composite materials. The main functions of the bipolar plates are current and heat conduction, distributing the reactant gases, as well as providing mechanical stability. Arguably, the properties of graphite composites are not optimal for these purposes. Graphite composites have only moderately high electrical or thermal conductivities and mechanical stability; the main reason they are used is their corrosion resistance. Metals provide much better properties except that they are prone to corrosion in a typical fuel cell environment. However, the corrosion resistance of metal bipolar plates can be improved by coating or surface modification, as reviewed extensively in Refs. [29–34]. If metallic bipolar plates were used, the thickness can be reduced to 0.1–0.2 mm, reducing weight by an order of magnitude. This would lead to a 3.5-fold increase in stack power density. Together with weight reductions of peripherals (end plates, screws, etc.), which account for 10–15% of the weight of the stack, a 5-fold increase in stack power density towards >10 kW/kg seems a reasonable estimate for future development, especially considering the above-mentioned improvements in catalyst layers.

The resulting mass of a propulsion energy system employing such a tailored tank and future lightweight fuel cell is presented in Table 2. As a reference, a current Airbus A320 (Airbus AG, Leiden, The Netherlands) is used, which would need 6980 kg kerosene for the study flight mission leading to a tank system of 9187 kg [16]. The two CFM-56-5A3 jet engines with 2331 kg each complete the energy system of the A320, yielding a total mass of 13849 kg. Table 2 reveals that an energy system employing current fuel cell technology would nearly double this mass. However, if the improvements in aircraft technology estimated by Liu et al. [19] are taken into account, the required power would reduce from 27.6 to 16.3 MW, which would reduce the mass of the fuel cell system to similar values of current combustion systems. If the future light-weight, high-power fuel cell technology discussed above would power current aircraft, the mass of the energy system could be reduced by 22%. Combining future aircraft technology with future fuel cell technology could lead to a mass reduction by 41%.

Table 2. Comparison of fuel cell system weight of current and future aircraft technology employing current and future fuel cell and electric motor (EM) technology.

Aircraft Tech., P_{rq}	Current FCS	Future FCS
	1.6 kW/kg FC 5.8 kW/kg EM	8 kW/kg FC 10 kW/kg EM
current, 27.6 MW	25,028 kg	10,900 kg
future, 16.3 MW	16,758 kg	8197 kg

FCS = fuel cell system.

Note that these mass reductions are estimated for one specific medium-haul mission. If the range of the mission changes, the power-to-energy ratio changes as well. Generally speaking, on short-range missions, the weight of the energy converter, i.e., fuel cell or jet engine, is more dominating. This leads to disadvantages for fuel cell systems compared to jet engines. On long-haul missions, the gravimetric energy density of the energy storage, i.e., the tank system, is determining. This puts hydrogen operated fuel cells at an advantage. These trends are shown in the Ragone plots in Figure 7. For short-haul flights, e.g., in the range of the 1 h line, only the future fuel cell system can compete with the current kerosene-fuelled jet engine. On long haul flights, e.g., along the 10 h line, the jet engine has higher power and energy densities than the current fuel cells with current tank technology. However, improving the tank technology already leads to a fuel cell energy system that is competitive with current jet engines. Improving the fuel cells further leads to higher power and energy densities, an advantage that is more pronounced the longer the flight mission is (cf. 1 h vs. 10 h line).

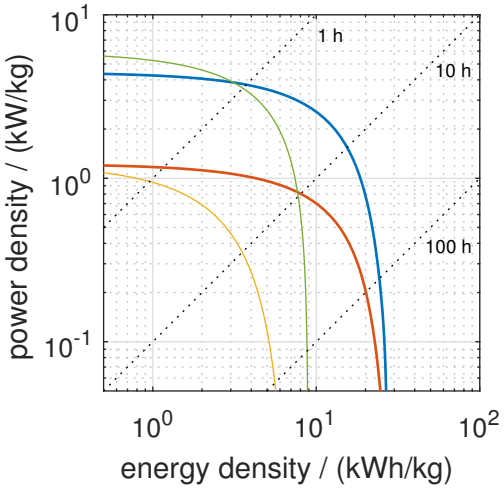

Figure 7. Ragone plot of current and future fuel cell systems for aviation. Yellow: current fuel cells with 1.6 kW/kg incl. periphery, current electric engines with 5.2 kW/kg and simple stationary tanks. Red: current fuel cells+periphery and electric engines with LH2 tanks optimized for medium-haul flight. Blue: future lightweight, high-power fuel cells+periphery with 8 kW/kg, future electric engines with 10 kW/kg and optimized LH2 tanks. Green: current system of jet engine (Airbus A320) and kerosene tanks. Dotted lines mark time constants of 1 h (top), 10 h (middle), and 100 h (bottom).

4. Conclusions

In this paper, the design of fuel cells for the main energy supply of passenger transportation aircraft is discussed. For the description of the behaviour of the fuel cell, a physical model covering the main electrochemical and transport processes was employed. The model uses effective physical parameters, which allows for estimating future materials' developments. From the general model-based analysis, it was seen that the optimal size of the fuel cell depends on the interplay of efficiency and power density. In any case, an oversizing of the fuel cell (or correspondingly operation below the maximum power point) is beneficial, since it increases efficiency.

A universal cost–benefit curve yielding the efficiency gain upon reduction of the operating power was derived. This curve proved to be insensitive to the parameters of the fuel cell and is thus of fundamental nature. To describe the trade-off between power and efficiency, a weight factor w_P was introduced, which allows for incorporating technical as well as non-technical design objectives into the design process of the fuel cell. Possible design objectives are system mass and volume, fuel burn and emissions, direct operating costs, carbon tax, emission targets or restrictions, social acceptance or hype of new technologies, political factors, and many more.

Applying the presented design process for weight optimization of a fuel cell system for passenger aircraft revealed that the optimal fuel cell size cannot be determined from the fuel cell model alone, but the characteristics of the other system components affect the optimal fuel cell design. Hence, the fuel cell needs to be designed in the context of the whole energy system. It was found that in systems in which the mass of the fuel cell is determining, the optimal oversizing of the cell is very small, whereas if the system is heavy in fuel and/or tank, it is beneficial to apply larger oversizing. Hence, the ratio of energy-to-power determines the optimal oversize of the stack.

The fuel cell model was combined with a detailed liquid hydrogen tank model, which maximizes the energy density towards a specific desired flight mission. Such a tailored tank design significantly reduces the tank mass and allows reaching energy densities of the tank system surpassing that of kerosene. This mass advantage of the tank system can compensate mass disadvantages of the other components, like the power densities of current fuel cells and electrical engines that fall behind jet engines.

Similarly to the tank, the future potential for lightweight fuel cell developments was discussed. While in the automotive sector, power density goals are already reached and are thus out of the focus of current research and development efforts, the power density of future fuel cell stacks could be improved by a factor of at least 5. Key components are the bipolar plates and peripheral components like end plates, which could be made from better performing, lightweight materials. Further improvements can be achieved with advanced catalyst designs. With these estimates, the total mass of fuel cell systems for passenger aircraft employing both current and future fuel cell technologies was determined. While current fuel cell technology can power aircraft, future technologies have the potential for mass reductions compared to jet engine technology. This advantage is especially pronounced in fuel-heavy aircraft like long haul aircraft.

The current design process focuses on the main components, i.e., fuel cell and hydrogen tank. Other fuel cell system components, especially hydrogen recycling, air supply and conditioning have been neglected. Furthermore, the overall system design has to consider not only weight, but also feasibility for dynamic and robust operation. Additionally, system integration into the airplane, including heat management, reactant supply and product usage, is an important step to increase overall efficiency. This remains a future task.

Acknowledgments: The authors would like to thank Tasleem Muzaffar for providing the fitting data of the experimental polarization curves used for the analysis in Figure 3. Additionally, we would like to thank Bekir Yildiz for providing the flight mission data used for the detailed tank design. Furthermore, the authors would like to acknowledge the support of the Ministry for Science and Culture of Lower Saxony (Grant No. VWZN3177) for funding the research project "Energy System Transformation in Aviation" in the initiative "Niedersächsisches Vorab".

Author Contributions: T.K. conceived the general design considerations and performed the analysis of the fuel cell model. C.W. conceived the detailed tank model and performed the detailed tank design. T.K. and C.W. conceived and designed the fuel cell system for future aircraft. All authors discussed the results and wrote and reviewed the manuscript. R.H.-R. and U.K. supervised the whole project.

Conflicts of Interest: The authors declare no conflict of interest.

Abbreviations

The following abbreviations are used in this manuscript:

CCL	Cathode catalyst layer
EM	Electric motor
FCS	Fuel cell system
GDL	Gas diffusion layer
MEA	Membrane electrode assembly
PEMFC	Polymer electrolyte membrane fuel cell

List of Symbols

b	Tafel slope, V
c_h	oxygen concentration in the channel, mol cm^{-3}
D	effective diffusion coefficient, cm^2 s^{-1}
E_rq	required energy
f	objective function
ΔG	Gibbs free energy
ΔH	reaction enthalpy
i_*	volumetric exchange current density, A cm^{-3}
j	local current density, A cm^{-2}
j_0	cell current density, A cm^{-2}
l	thickness, m
m	mass, kg
P_rq	required power

r	ratio, dimensionless
R_Ω	ohmic resistance, Ω
w_P	weight parameter w.r.t power

Greek

η	local overpotential, V
η_0	cell overpotential, V
ρ_{fc}	specific power of the fuel cell, kW kg^{-1}
ϱ_{tk}	area-specific tank mass, kg m^{-2}
σ_{t}	proton conductivity in the catalyst, S m^{-1}
v	efficiency
$\omega_{\mathrm{H_2}}$	specific energy of hydrogen, 33.3 kWh kg^{-1}

Subscripts and Superscripts

b	backing or gas diffusion layer
c	converter
fc	fuel cell
m	membrane
max	maximum
oc	open circuit
os	oversize
rq	required
s	storage
t	cathode catalyst layer
tk	tank

Appendix A. Mass of a Spherical Tank

$$\begin{aligned} m_{\mathrm{tk}} &= \varrho_{\mathrm{tk}} A_{\mathrm{tk}} \\ &= 4\pi r^2, \end{aligned} \tag{A1}$$

with

$$r^3 = \frac{3}{4\pi} V, \tag{A2}$$

$$\begin{aligned} m_{\mathrm{tk}} &= \varrho_{\mathrm{tk}} 4\pi \left(\frac{3}{4\pi} V\right)^{\frac{2}{3}} \\ &= \varrho_{\mathrm{tk}} (\pi)^{\frac{1}{3}} \left(6 \frac{E_{\mathrm{rq}}}{\omega_{\mathrm{H_2}} v \rho_{\mathrm{H_2}}}\right)^{\frac{2}{3}}. \end{aligned} \tag{A3}$$

References

1. International Energy Agency. *CO_2 Emissions From Fuel Combustion: Highlights 2017*; Technical Report; International Energy Agency: Paris, France, 2017.
2. Air Transport Action Group. *Aviation Benefits Beyond Borders*; Technical Report; Air Transport Action Group: Geneva, Switzerland, 2016.
3. Darecki, M.; Edelstenne, C.; Enders, T.; Fernandez, E.; Hartman, P.; Herteman, J.P.; Kerkloh, M.; King, I.; Ky, P.; Mathieu, M.; et al. *Flightpath 2050*; Technical Report; European Commission: Brussels, Belgium, 2011.
4. Müller, C.; Kieckhäfer, K.; Spengler, T.S. The influence of emission thresholds and retrofit options on airline fleet planning: An optimization approach. *Energy Policy* **2018**, *112*, 242–257.

5. Bockris, J.; Justi, E.W. *Wasserstoff—Energie für alle Zeiten*; Pfriemer Verlag: München, Germany, 1980.
6. Brewer, G.; Morris, R. *Study of LH2 Fueled Subsonic Passenger Transport Aircraft*; Technical Report, NASA CR-144935; NASA: Washington, DC, USA, 1976.
7. Khandelwal, B.; Karakurt, A.; Sekaran, P.R.; Sethi, V.; Singh, R. Hydrogen powered aircraft: The future of air transport. *Prog. Aerosp. Sci.* **2013**, *60*, 45–59.
8. Verstraete, D. Long range transport aircraft using hydrogen fuel. *Int. J. Hydrogen Energy* **2013**, *38*, 14824–14831.
9. Friedrich, K.A.; Kallo, J.; Schirmer, J.; Schmitthals, G. Fuel Cell Systems for Aircraft Application. *ECS Trans.* **2009**, *25*, 193–202.
10. Jenssen, D.; Berger, O.; Krewer, U. Improved PEM fuel cell system operation with cascaded stack and ejector-based recirculation. *Appl. Energy* **2017**, *195*, 324–333.
11. Zenith, F.; Weinzierl, C.; Krewer, U. Model-based analysis of the feasibility envelope for autonomous operation of a portable direct methanol fuel-cell system. *Chem. Eng. Sci.* **2010**, *65*, 4411–4419.
12. Na, Y.; Zenith, F.; Krewer, U. Highly integrated direct methanol fuel cell systems minimizing fuel loss with dynamic concentration control for portable applications. *J. Process Control* **2017**, *57*, 140–147.
13. Kulikovsky, A.A. A Physically-Based Analytical Polarization Curve of a PEM Fuel Cell. *J. Electrochem. Soc.* **2014**, *161*, F263–F270.
14. Perry, M.L.; Newman, J.; Cairns, E.J. Mass Transport in Gas-Diffusion Electrodes: A Diagnostic Tool for Fuel-Cell Cathodes. *J. Electrochem. Soc.* **1998**, *145*, 5–15.
15. Eikerling, M.; Kornyshev, A. Modelling the performance of the cathode catalyst layer of polymer electrolyte fuel cells. *J. Electroanal. Chem.* **1998**, *453*, 89–106.
16. Winnefeld, C.; Kadyk, T.; Krewer, U.; Hanke-Rauschenbach, R. Modelling and Designing Cryogenic Hydrogen Tanks in Terms of Aircraft Applications. *Energies* **2018**, *11*, 105.
17. Leachman, J.W.; Jacobsen, R.T.; Penoncello, S.G.; Lemmon, E.W. Fundamental equations of state for parahydrogen, normal hydrogen, and orthohydrogen. *J. Phys. Chem. Ref. Data* **2009**, *38*, 721–748.
18. Dobson, P.; Lei, C.; Navessin, T.; Secanell, M. Characterization of the PEM Fuel Cell Catalyst Layer Microstructure by Nonlinear Least-Squares Parameter Estimation. *J. Electrochem. Soc.* **2012**, *159*, B514–B523.
19. Liu, Y.; Elham, A.; Horst, P.; Hepperle, M. Exploring vehicle level benefits of revolutionary technology progress via aircraft design and optimization. *Energies* **2018**, *11*, 166.
20. Linde A.G.. *Cryogenic Standard Tanks*; Technical Report; Linde AG: Tacherting, Germany, 2016.
21. Intelligent Energy Ltd. *Ultra Lightweight Fuel Cell Systems—UAV Application Guide*; Technical Report; Intelligent Energy Ltd.: Loughborough, UK, 2016.
22. Siemens A.G. *Factsheet Rekord-Motor SP260D und Extra 330LE*, Technical Report; Siemens AG: München, Germany; 2017.
23. Muzaffar, T.; Kadyk, T.; Eikerling, M. Tipping Water Balance in Polymer Electrolyte Fuel Cells with Ultra-Low Pt Loading. *Energy Environ. Sci.* **2017**, submitted.
24. United States Department of Energy. *Fuel Cell Technologies Office Multi-Year Research, Development, and Demonstration Plan, 2016 Fuel Cells Section*; Technical Report; United States Department of Energy: Washington, DC, USA, 2016.
25. Eslamibidgoli, M.J.; Huang, J.; Kadyk, T.; Malek, A.; Eikerling, M. How theory and simulation can drive fuel cell electrocatalysis. *Nano Energy* **2016**, *29*, 334–361.
26. Klingele, M.; Breitwieser, M.; Zengerle, R.; Thiele, S. Direct deposition of proton exchange membranes enabling high performance hydrogen fuel cells. *J. Mater. Chem. A* **2015**, *3*, 11239–11245.
27. Yoshida, T.; Kojima, K. Toyota MIRAI Fuel Cell Vehicle and Progress Toward a Future Hydrogen Society. *Interface Mag.* **2015**, *24*, 45–49.
28. Tsuchiya, H.; Kobayashi, O. Mass production cost of PEM fuel cell by learning curve. *Int. J. Hydrogen Energy* **2004**, *29*, 985–990.
29. Hermann, A.; Chaudhuri, T.; Spagnol, P. Bipolar plates for PEM fuel cells: A review. *Int. J. Hydrogen Energy* **2005**, *30*, 1297–1302.
30. Yuan, X.Z.; Wang, H.J.; Zhang, J.J.; Wilkinson, D.P. Bipolar plates for PEM fuel cells—From materials to processing. *J. New Mater. Electrochem. Syst.* **2005**, *8*, 257–267.
31. Tawfik, H.; Hung, Y.; Mahajan, D. Metal bipolar plates for PEM fuel cell-A review. *J. Power Sources* **2007**, *163*, 755–767.

32. Antunes, R.A.; Oliveira, M.C.L.; Ett, G.; Ett, V. Corrosion of metal bipolar plates for PEM fuel cells: A review. *Int. J. Hydrogen Energy* **2010**, *35*, 3632–3647.
33. Wang, H.; Turner, J.A. Reviewing metallic PEMFC bipolar plates. *Fuel Cells* **2010**, *10*, 510–519.
34. Karimi, S.; Fraser, N.; Roberts, B.; Foulkes, F.R. A review of metallic bipolar plates for proton exchange membrane fuel cells: Materials and fabrication methods. *Adv. Mater. Sci. Eng.* **2012**, *2012*, 828070, doi:10.1155/2012/828070.